RESEARCH ARTICLE

Processes controlling aggregate formation and distribution during the Arctic phytoplankton spring bloom in Baffin Bay

Jordan Toullec[1,*], Brivaëla Moriceau[1], Dorothée Vincent[2], Lionel Guidi[3], Augustin Lafond[4], and Marcel Babin[5,6]

In the last decades, the Arctic Ocean has been affected by climate change, leading to alterations in the sea ice cover that influence the phytoplankton spring bloom, its associated food web, and therefore carbon sequestration. During the Green Edge 2016 expedition in the central Baffin Bay, the phytoplankton spring bloom and its development around the ice edge was followed along 7 transects from open water to the ice-pack interior. Here, we studied some of the processes driving phytoplankton aggregation, using aggregate and copepod distribution profiles obtained with an underwater vision profiler deployed at several stations along the transects. Our results revealed a sequential pattern during sea ice retreat in phytoplankton production and in aggregate production and distribution. First, under sea ice, phytoplankton started to grow, but aggregates were not formed. Second, after sea ice melting, phytoplankton (diatoms and *Phaeocystis* spp. as the dominant groups) benefited from the light availability and stratified environment to bloom, and aggregation began coincident with nutrient depletion at the surface. Third, maxima of phytoplankton aggregates deepened in the water column and phytoplankton cells at the surface began to degrade. At most stations, silicate limitation began first, triggering aggregation of the phytoplankton cells; nitrate limitation came later. Copepods followed aggregates at the end of the phytoplankton bloom, possibly because aggregates provided higher quality food than senescing phytoplankton cells at the surface. These observations suggest that aggregation is involved in 2 export pathways constituting the biological pump: the gravitational pathway through the sinking of aggregates and fecal pellets and the migration pathway when zooplankton follow aggregates during food foraging.

Keywords: Arctic phytoplankton spring bloom, Baffin Bay, Sea ice, Diatoms, *Phaeocystis* spp., Copepods, Marine snow, Aggregates, UVP5

Introduction

The thickness and areal extent of sea ice in the Arctic Ocean have changed dramatically in recent decades due to global warming (Comiso, 2002; Stroeve et al., 2007; Comiso et al., 2008; Kwok and Rothrock, 2009; Screen and Simmonds, 2010; Vihma, 2014). The consequences for marine ecosystems remain difficult to predict. Furthermore, in this context, the Arctic Ocean exerts a feedback on global climate (Masson-Delmotte et al., 2018). Sea ice is an essential component of global biogeochemical cycles in polar ecosystems and supports polar marine food webs (Vancoppenolle et al., 2013). Ice-algal and phytoplankton blooms begin when light intensity and nutrient concentrations are sufficient (e.g., Tremblay et al., 2006; Assmy et al., 2017). The resulting biomass is controlled by additional factors such as coupling with grazer life cycles (Søreide et al., 2010; Leu et al., 2011) and ocean surface temperature (Feng et al., 2016). Phytoplankton blooms typically occur after ice melt when the water column is stratified (Søreide et al., 2010; Randelhoff et al., 2019). The succession of ice-algal and phytoplankton blooms, within and beneath the sea ice, determines the reproduction and growth of grazers (Søreide et al., 2010: Leiknes et al.,

[1] Univ Brest, CNRS, IRD, Ifremer, Laboratoire des sciences de l'environnement marin (LEMAR), Plouzané, France

[2] Office Français de la Biodiversité (OFB), Direction Surveillance, Evaluation Données (DSUED), Service Évaluation Connaissances et Usages du Milieu Marin (ECUMM), Brest, France

[3] Sorbonne Universités, UPMC Université Paris 06, CNRS, Laboratoire d'Océanographie de Villefranche (LOV) UMR7093, Observatoire Océanologique, Villefranche-sur-Mer, France

[4] Aix-Marseille University, Université de Toulon, CNRS, IRD, MIO, UM 110, Marseille, France

[5] Takuvik Joint International Laboratory, Laval University (Québec City, Quebec, Canada), Centre National de la Recherche Scientifique (CNRS), Paris, France

[6] Département de biologie et Québec-Océan, Université Laval, Québec City, Quebec, Canada

* Corresponding author:
Email: toullec.jordan@gmail.com

2016). Ice algae are grazed by small planktonic crustaceans (e.g., krill and copepods), which in turn are preyed upon by higher trophic levels such as fish, birds, and mammals (Nielsen and Hansen, 1995; Hansen et al., 1996; Darnis et al., 2008; Darnis et al., 2012; Darnis et al., 2017). Unconsumed organic matter produced within and beneath the ice descends into the water column as senescent algae, aggregates, appendicular houses, or fecal pellets (Forest et al., 2018). Depending on the depth reached (Kellogg et al., 2011), this organic matter can either be consumed by benthic feeders, buried in the sediment, or sequestered over long periods of time in deep water (Leu et al., 2011; Wassmann et al., 2011; Forest et al., 2018).

With the decline of sea ice in recent decades, a decrease in the total amount of organic matter produced in the ice is expected, due to the loss of habitat for sympagic algae (primary producers associated with the ice), with a possible collapse of the entire food web and associated biogeochemical processes underneath the sea ice (Arrigo and Dijken, 2011; Arrigo, 2014; Babin, 2020). Early spring sea ice breakup will affect the timing of summer phytoplankton blooms and may result in a lag between ice algae and phytoplankton blooms, which may have a significant impact on copepod reproductive success and subsequent biomass (Søreide et al., 2008; Søreide et al., 2010; Søreide et al., 2013; Janout et al., 2016) and affect the entire pelagic food web after sea ice retreat (Tedesco et al., 2019).

Baffin Bay, located at the gateway to the Arctic Ocean, is a heterogeneous environment with two different currents flowing in opposite directions: a warm, salty current from the southeast and a cold current from the northern Arctic that flows along the west coast of Baffin Bay (Tang et al., 2004). The circulation affects the stratification regime and the biogeochemical environment of Baffin Bay, which controls phytoplankton community production and structure and, in the end, carbon transfer through the planktonic food web (Saint-Béat et al., 2020). The bay is completely ice-covered from December to March. During the Arctic spring, due to ice retreat, light passes through the water column and nutrient-rich waters flow into the bay. Nutrient-rich Atlantic waters from the Greenland Current (Torres-Valdés et al., 2013), nutrient-rich waters from the Canadian Archipelago (Coachman and Aagaard, 1974; Newton et al., 1974), and nutrient flux from depth, through remineralization and its vertical input due to mixing, provide nutrients to Baffin Bay (Tremblay et al., 2002; 2006). The combination of light, nutrients, and increased stratification creates a stable environment for phytoplankton growth in the water column around May (Massicotte et al., 2018; Massicotte et al., 2019; Oziel et al., 2019; Randelhoff et al., 2019). Diatoms and *Phaeocystis* spp. are the dominant components of the phytoplankton assemblage in the turbulent, nutrient-rich waters in spring (Smith et al., 1991; Rousseaux and Gregg, 2013). The contribution of *Phaeocystis* spp. to spring blooms may increase with global change, as nutrient limitations and inflow from Atlantic waters may increase (Marchant and Thomsen, 1994; Gabric et al., 2003; Schoemann et al.,

2005). Isolated phytoplankton cells are generally remineralized by microbial activity or consumed by zooplankton at the ocean surface. Diatoms and *Phaeocystis* spp. can also aggregate into large particles that sink at the end of the phytoplankton bloom (Smith et al., 1991; Riebesell, 1993; Riebesell et al., 1995; Mari et al., 2005; Cavan et al., 2019; Henson et al., 2019; Prairie et al., 2019). Due to their rapid sedimentation rates, these aggregates typically drive vertical export (Moriceau et al., 2007; Turner, 2015). The succession of ice-algal and pelagic blooms and their fate through higher trophic levels and vertical transfer remain poorly understood.

To understand and predict carbon export in the Arctic Ocean, we need to understand the parameters that trigger aggregation in the Arctic spring phytoplankton bloom. The Green Edge project was developed to (1) study the timing and development of the Arctic spring phytoplankton bloom, (2) understand the fate of the organic matter produced, and (3) improve our understanding of the polar ecosystem in a changing climate. This study, focusing on the fate of the Arctic spring bloom, benefited from the large data set collected during the 2016 Green Edge expedition in Baffin Bay. In an effort to highlight the role of phytoplankton bloom dynamics and environmental biochemical conditions in macroaggregate (marine snow) formation and distribution, this large data set was linked to particle and zooplankton abundance profiles collected with an Underwater Video Profiler 5 (UVP5).

Methods
Sampling area
The Green Edge expedition onboard the icebreaker CCGS *Amundsen* was conducted from June 9 to July 10, 2016, in Baffin Bay. A total of 7 transects with 137 stations crossing an area from 55°W to 64°W and from 67°N to 71°N were visited (**Figure 1**).

Sea ice satellite data and open water days
Sea ice concentration (SIC) is an index that ranges from 0 (for complete open water) to 1 (for full ice cover). SIC data were extracted from AMSR2 radiometer daily data on a 3.125-km grid (Beitsch et al., 2014). At each station, the SIC was extracted from the closest pixel using the Euclidean distance between the ship position and the center of each pixel. In this study, a site was considered free of ice when the SIC was less than 50% (where 0% is ice-free open water, and 100% is totally ice-covered). For each sampling station and at each sampling moment, the number of open water days (OWD) was computed. OWD corresponds to the number of days since the site became ice-free (positive values) or before the ice melt (negative values).

Depth of the euphotic zone
For each station, the depth of the euphotic zone, *Ze*, was defined as the depth where a daily irradiance of photosynthetically available radiation reached 0.415 mol photons m^{-2} d^{-1} (Lafond et al., 2019; Massicotte et al., 2019; Randelhoff et al., 2019).
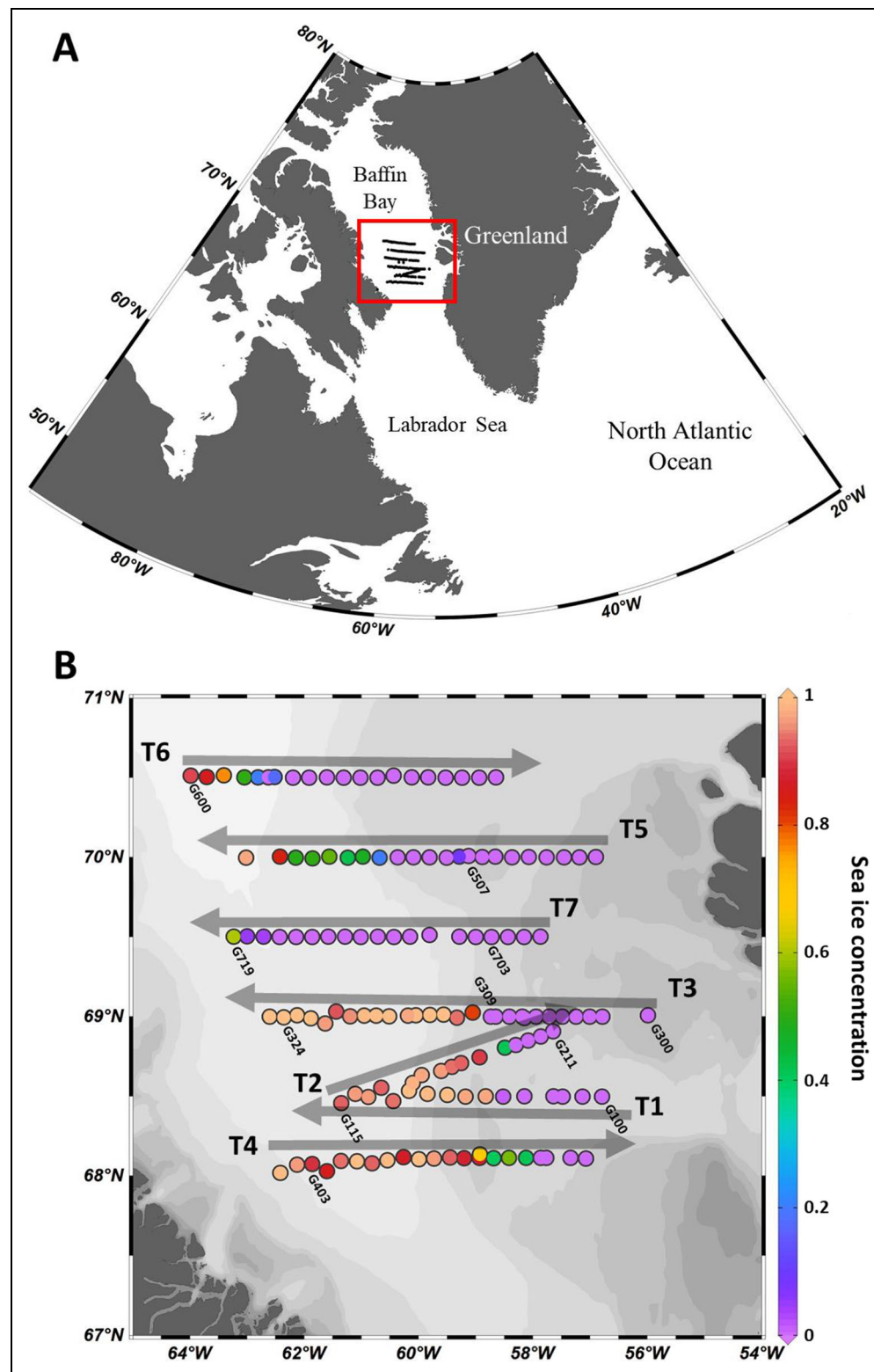
Figure 1. Map of study area showing transects, stations sampled, and sea ice concentration. (A) Study area in Baffin Bay during the Green Edge cruise aboard the *Amundsen*. (B) Zoom of the red square in (A), where black dashed arrows represent the 7 transects, ordered chronologically, and the ship's direction. Each dot corresponds to a sampling station for a total of 137 hydrological stations. Color scale corresponds to the sea ice concentration (areal fraction that was ice-covered) at each station. DOI: https://doi.org/10.1525/elementa.2021.00001.f1

Equivalent mixing layer (EML) consideration

In Baffin Bay during the Green Edge 2016 expedition, the depth of the EML was shallow (17 to 30 m) depending on freshwater inputs due to ice melting (Randelhoff et al., 2019). This variation was neglected in our analysis, and surface data were averaged over

a fixed EML of 30 m, the maximum mixing layer depth in Randelhoff et al. (2019).

Analysis of water samples

Seawater was collected, using a rosette of Niskin bottles, at 7–14 different depths. At each hydrographic station, vertical profiles of water column properties were made using a conductivity–temperature–depth (CTD) sensor system (Seabird SBE-911 plus), installed onboard the CCGS *Amundsen*, which also included a Seapoint SCF Fluorometer for detection of chlorophyll *a*, and a WetLabs C-Star transmissometer to measure beam attenuation as an indicator of biomass. Water samples were collected as the Niskin bottles were brought up to depths determined using data collected by the CTD upon descent.

Dissolved nutrients

Nutrient (NO_3^-, HPO_4^{3-}, and H_4SiO_4) concentrations were measured at 44 stations covering the 7 transects (Table S1). Samples were taken from surface to depth with bathymetry ranging from 350 to 2000 m. Analyses were performed onboard on a Bran + Luebbe Autoanalyzer 3 using standard colorimetric methods (Grasshoff et al., 2009). Analytical detection limits were 0.03 μM for NO_3^-, 0.05 μM for PO_4^{3-}, and 0.1 μM for H_4SiO_4.

Biogenic silica

Biogenic silica (bSi) concentrations were measured at 28 stations covering the 7 transects (Table S1). Samples were taken at depths between 0 and 350 m with one deep profile going to a depth of 1,650 m. For each sample, 1 L of seawater was filtered onto 0.4 μm polycarbonate filters (Nucleopore Whatman). Filters were then stored in Eppendorf vials and dried for 24 h at 60°C before being stored at room temperature. bSi was measured by the hot NaOH digestion method of Paasche (1973) modified by Nelson et al. (1989), with an analytical detection limit of 0.005 μM.

Phytoplankton identification and counting

Identification and quantitative assessment of phytoplankton communities were carried out on 43 samples from the surface (depth of 0–2 m) and the subsurface chlorophyll *a* maximum (SCM, depth of 15–44 m) at 24 stations (Table S1). The SCM was identified using a Seapoint SCF Fluorometer for detection of chlorophyll *a*. Aliquots of 25–50 mL were preserved with 0.8 mL Lugol iodine solution in dark glass bottles and then stored in the dark at 4°C until analysis. For each sample, microscopic counts and identifications were made in the laboratory following the Utermöhl settling method (1958). Counts were performed by inverted microscopy (Nikon Eclipse TS100; Utermöhl, 1958). A minimum of 400 phytoplankton cells per sample were counted at 100 magnification (see Lafond et al., 2019, for further details). As they constitute the major components of the Arctic ecosystem, diatoms (Baccilariophyceae) and *Phaeocystis* spp. (Prymnesiophyceae) were studied as the priority. Diatom carbon biomass (μg C L^{-1}) was estimated following the method provided by Lafond et al. (2019; their table S3). Concerning *Phaeocystis* spp., cell

abundance (Green Edge Dataset, 2021) was converted to biomass (μg C L^{-1}) assuming a carbon cell content of 14.2 pg C cell^{-1} (Rousseaux et al., 1990).

Pigments

For pigments, 521 samples were analyzed from 52 stations covering 7 transects (Table S1). About 2.7-L seawater samples were filtered onto 0.7-μm pore size Whatman GF/F filters and stored in liquid nitrogen prior to analysis. Then, filters were extracted in 100% methanol, disrupted by sonication, and clarified by filtration (GF/F Whatman). Samples were analyzed the same day using high-performance liquid chromatography with an Agilent Technologies HPLC 1200 system with diode array and fluorescence detection (Ras et al., 2008).

Particles and zooplankton distribution

The vertical distribution of large particulate matter (>600 μm to 2 cm) was studied using a nondestructive imaging system, the UVP5 (Picheral et al., 2010). The UVP5 was mounted on the CTD-rosette frame and positioned at the lowest location in order to profile minimally disturbed water during descent. The UVP5 deployments were undertaken on 137 hydrologic stations, from the surface to the bottom depth, and a total of 196 vertical profiles covering 7 transects were performed during the cruise (Table S1).

Images recorded by the UVP5 were processed with custom-developed image analysis software and extracted using the ZooProcess® software (Gorsky et al., 2010). Using the ECOTAXA 2.0 software, for all images, the major and minor axes of each object were measured and converted into biovolume (mm^3) assuming that the particle-projected shape was ellipsoid. A computer-assisted method was used to classify all organisms in groups of vignettes using the Random Forest algorithm. Machine learning classification was subsequently verified manually. In this study, the concentration of marine snow aggregates and distribution of copepods were analyzed along with the 196 profiles at a 5-m depth resolution.

Marine snow aggregate image analyses

Marine snow aggregates were identified and characterized by irregular shape, their grainy appearance, and their heterogeneity of shape. In this study, long stick-shaped particles were disregarded as more representative of fecal pellets. The aggregate equivalent spherical diameter was calculated from the biovolume assuming that aggregates are prolate spheroid in shape (Hillebrand et al., 1999).

Copepod image analyses

Copepod images (copepod vignettes including copepod-like subvignettes) were validated by taxonomic expertise considering that the prosome shape (lengthy ovoid) is about twice as long as the urosome and that the presence of 2 long and thin antennae that at least represented twice the prosome length could be affiliated to copepod vignette. For the UVP images of copepods ranging from 0.7 to 7 mm, the resolution was not adequate to distinguish copepod species or developmental stages. In Arctic environments, zooplankton communities are dominated
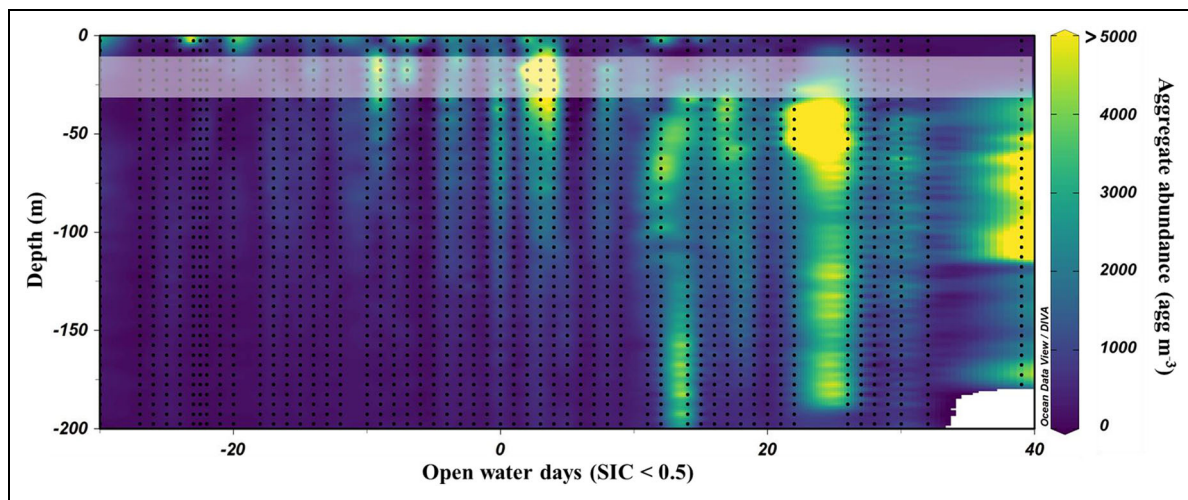
Figure 2. Vertical profiles of aggregate abundance by open water days. Aggregate abundance (agg m^{-3}), pooled from 137 hydrological stations, is indicated by color-coding. On the *x*-axis, open water days correspond to number of days since the site became ice-free (positive values) or before the ice melt (negative values), where ice-free is defined as sea ice concentration below 50% (SIC < 0.5). The horizontal shaded area represents the upper and lower depths of the equivalent mixing layer estimated by Randelhoff et al. (2019) during the *Amundsen* cruise. Black dots correspond to Underwater Video Profiler 5 profiles. DOI: https://doi.org/10.1525/elementa.2021.00001.f2

by only a few copepod species such as *Calanus glacialis* and *Calanus finmarchicus*, *Calanus hyperboreus*, *Metridia longa*, and *Pseudocalanus* spp. adults (Vilgrain et al., 2021).

Principal component analysis (PCA)

To describe and relate biogeochemical parameters to aggregate abundance, we performed a PCA (Legendre and Legendre, 2012). We included the following parameters, all of which were available concurrently for 28 stations: the biogeochemical parameters of EML nitrate, phosphate, and silicate concentrations; the biological parameters of EML copepod abundance and bSi, chlorophyll *a*, and phaeopigment concentrations, surface and SCM biomass of diatoms and *Phaeocystis* spp., and maximum depth of copepod abundance; and the aggregate distributional characteristics of EML aggregate abundance, depth-integrated (30–200 m) aggregate abundance, and depth of maximum aggregate abundance. The 28 stations were clustered by hierarchical classification on the coordinates for the first 3 principal components, using Euclidean distance.

Results

Aggregate sizes and abundance

The aggregate equivalent spherical diameter ranged from 1 to 5 mm (mean $\pm$ standard error of 1.3 $\pm$ 0.2 mm, $n =$ 25,649) with corresponding biovolume ranging between 0.60 and 78.9 mm^3 (mean of 1.04 $\pm$ 0.01 mm^3). No variation in the aggregate size spectra among transects was detected, nor did the average aggregate size change with depth or with the progressive aging of the bloom from the ice edge to the open water stations. When plotted against OWD, the profiles of aggregate abundance illustrate the progressive deepening of the aggregates (**Figure 2**). Aggregate abundances were at a maximum at the surface when sea ice was still present (OWD < −

10) and between 13 and 30 m for OWD ranging from −10 to 11. As OWD increased further, several profiles showed high aggregate abundances distributed between depths of 50 and 200 m with large abundances just below the maximum mixed layer depth. Higher abundances (>5,000 aggregates m^{-3}) were recorded below this depth after the ice melt (**Figure 2**).

Aggregates and nutrient limitations

Average nitrate, silicate, and phosphate concentrations in the EML (first 30 m) were higher in stations under the ice (OWD < 0). Nitrate concentrations varied between 2 and 6 μM, silicate concentrations between 2 and 10 μM, and phosphate concentrations between 0.2 and 0.8 μM. After ice melting, represented by OWD from 0 to 30, nitrate concentrations rapidly approached 0 μM in 2–10 days depending on the station, while concentrations of silicate dropped to 1 μM and phosphate to 0.2 μM (Table S1; **Figure 3**). After 10 days free of ice, most stations were totally depleted of nitrate; after 20 ice-free days, most stations were totally depleted of silicate. **Figure 3** shows the progressive nutrient depletion from stations under the sea ice (OWD < 0) to open water stations (OWD > 0), with an intensification of the depletion around the ice edge, confirming that nutrient uptake by the phytoplankton community strongly depleted nutrient stocks in surface waters. Aggregate abundance in the EML was highest around OWD = 0. The highest aggregate abundances were recorded concurrently at stations where silicate concentrations were lower than 2 μM. At these stations, nitrate and phosphate concentrations were more variable, ranging between 0 and 5 μM for nitrate and 0.1 and 0.4 μM for phosphate. After more than 5 days free of ice, aggregate maxima appeared below the mixed layer. This evidence of aggregate sinking can explain why the aggregate abundance at the surface around the ice edge at these stations
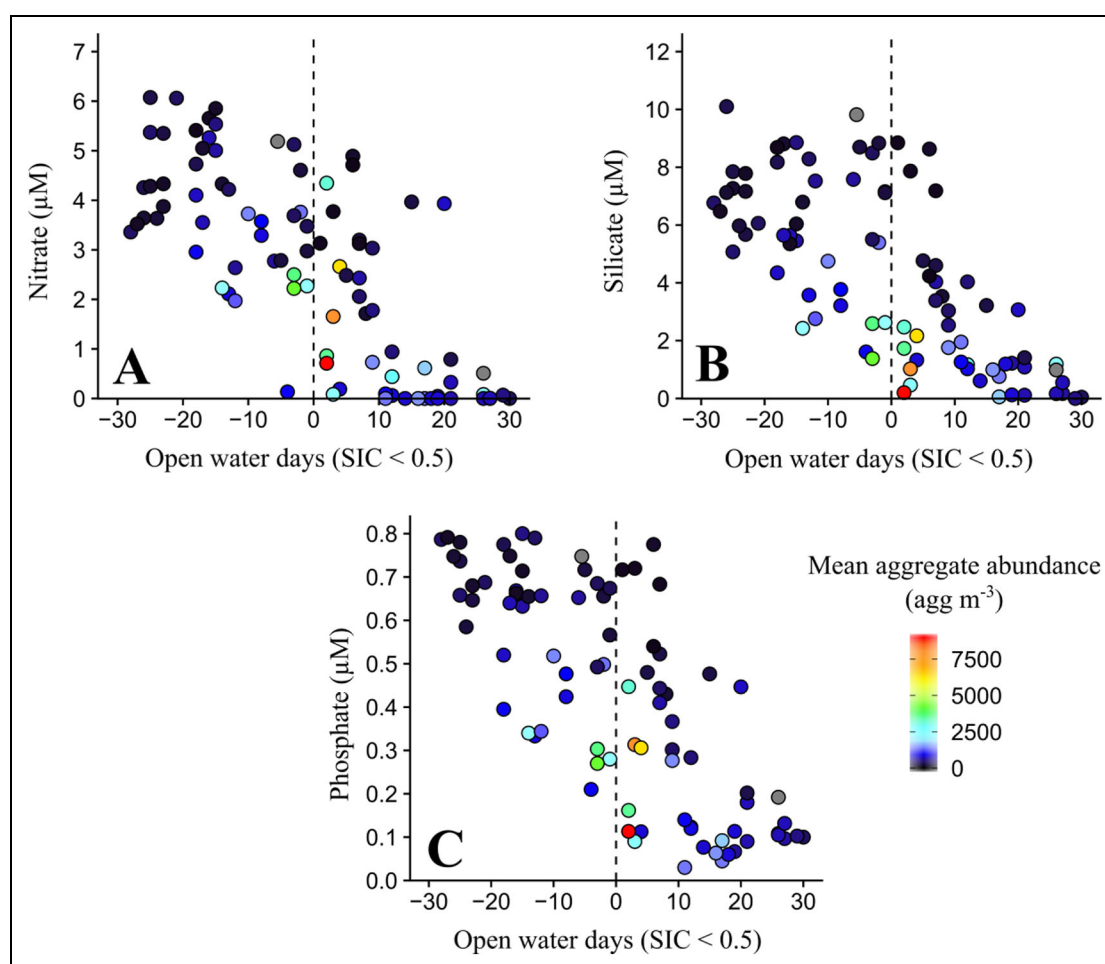
Figure 3. Nutrient concentrations and aggregate abundance by open water days. Depicted on the *y*-axes are the mean nutrient concentrations (μM) in the equivalent mixed layer (EML, 30-m depth) for (A) nitrate, (B) silicate, and (C) phosphate for 44 hydrological stations. On the *x*-axes, open water days correspond to number of days since the site became ice-free (positive values) or before the ice melt (negative values), where ice-free is defined as sea ice concentration below 50% (SIC < 0.5). Station data (solid circles) are color-coded for mean aggregate abundance (agg m^{-3}) in the EML. DOI: https://doi.org/10.1525/elementa.2021.00001.f3

was as low as it was prior to detecting aggregate formation.

Aggregate distribution and phytoplankton species

Phaeocystis spp. and diatoms constituted the bulk of phytoplankton stocks in both abundance and biomass (**Table 1**) at the two sampled depths: the surface (0–5 m) and the SCM. Concentrations of *Phaeocystis* spp. ranged from 2.8 $\times$ 10^3 to 11.5 $\times$ 10^6 cells L^{-1} (with biomass ranging from 0.04 to 163 μg C L^{-1}), whereas diatom concentrations ranged from 1 $\times$ 10^3 to 9 $\times$ 10^5 cell L^{-1} (with biomass ranging from 0.1 to 210 μg C L^{-1}). Cell abundance in the surface was higher for *Phaeocystis* spp. than for diatoms, but due to their small size, *Phaeocystis* spp. represented lower biomass (18 $\pm$ 21 μg C L^{-1}, $n = 36$, vs. 30 $\pm$ 36 μg C L^{-1}, $n = 44$, for diatoms). Cell concentrations of both diatoms and *Phaeocystis* spp. increased simultaneously and reached maxima around OWD = 0, when the ice was melting. Microscopy revealed that diatoms were the main silicifiers (Lafond et al., 2019), validating the use of bSi as a proxy for diatom abundance in this study.

High bSi concentrations and aggregate abundances were observed concurrently in the surface along transects T1, T3, and T5 (**Figures 4** and **5**). Along transect T3, a deep bSi concentration maximum (close to 1 μM) was observed below 100 m from West to East (**Figure 4**). At the same time, the maximum aggregate abundance was measured at 32.5-m depth at station G310 (7.2 $\times$ 10^3 aggregates m^{-3}). Close to the eastern part of the transect, deep aggregate concentrations were observed at 102.5 m at station G3000 (11.3 $\times$ 10^3 aggregates m^{-3}), and bSi concentrations were >0.5 μM (G3000 on T3; **Figure 4**). Within transect T1, we observed high aggregate abundance and low bSi concentration (<1 μM). Abundances higher than 1 $\times$ 10^3 aggregates m^{-3} were measured below a depth of 50 m and deepened from West to East (T1; **Figure 4**). While at some stations aggregate abundance may be associated with *Phaeocystis* spp. concentration, the highest aggregate abundances co-occurred with the highest bSi concentrations (up to 1.5 μM, at stations G204, G207, G309, G507, and G215; **Figure 5**). This trend was particularly evident during ice melting when the aggregates formed, with the exception

Table 1. Counts and biomass of the major phytoplankton groups in the surface and the subsurface chlorophyll maximum (SCM). DOI: https://doi.org/10.1525/elementa.2021.00001.t1

Station	Latitude (°N)	Longitude (°W)	SCM Depth (m)	Euphotic Depth (m)	Sample	*Phaeocystis* spp. (cell L^{-1})	(µg C L^{-1})	Diatoms (cell L^{-1})	(µg C L^{-1})
G100	68.499	56.790	40	41	Surface	na[a]	na	33,800	5.4
					SCM	na	na	34,480	9.4
G102	68.497	57.479	40	33	Surface	na	na	na	na
					SCM	na	na	47,960	16.7
G115	68.456	61.356	30	31	Surface	2,772	<0.1	24,700	1.4
					SCM	14,360	0.2	1,764	0.5
G201	68.633	59.947	40	31	Surface	11,340	0.2	19,660	3.7
					SCM	19,400	0.3	13,360	1.5
G204	68.708	59.257	15	22.5	Surface	2,063,000	29.3	915,600	93.6
					SCM	3,061,000	43.5	463,700	122.7
G207	68.794	58.529	15	22.5	Surface	2,352,000	33.4	78,630	26.5
					SCM	6,959,000	98.8	119,400	55.5
G300	68.999	56.789	44	na	Surface	29,230	0.4	16,130	6.8
					SCM	2,397,000	34	34,780	9.3
G309	69.000	58.739	15	29.5	Surface	400,400	5.7	256,500	36.2
					SCM	2,104,000	29.9	429,000	56.5
G312	69.012	59.562	15	15.8	Surface	78,370	1.1	18,900	3.4
					SCM	1,177,000	16.7	86,440	16.5
G318	69.007	60.953	na	27.5	Surface	na	na	8,920	1.2
					SCM	na	na	na	na
G324	68.996	62.358	20	21.5	Surface	85,930	1.2	48,130	5.7
					SCM	83,410	1.2	27,470	2.9
G403	68.031	61.601	na	40.5	Surface	na	na	18,680	1.2
					SCM	na	na	na	na
G409	68.106	59.994	na	27	Surface	na	na	30,000	4.2
					SCM	na	na	na	na
G413	68.123	58.966	30	na	Surface	75,850	1.1	21,670	7.1
					SCM	577,300	8.2	18,900	2.5
G418	68.114	57.770	30	43	Surface	24,440	0.3	1,008	0.1
					SCM	41,830	0.6	1,764	0.1
G507	70.009	59.124	12	20	Surface	172,400	2.4	624,000	149
					SCM	1,051,000	14.9	610,300	210
G512	70.000	60.362	15	21	Surface	568,000	8.1	204,600	70.3
					SCM	11,520,000	164	483,800	135.7
G600	70.511	63.988	na	28	Surface	na	na	204,600	70.3
					SCM	na	na	482,800	135.7
G605	70.503	62.517	20	41.5	Surface	5,544	0.1	30,490	5.9
					SCM	58,460	0.8	43,850	2.4
G615	70.499	59.525	30	30.5	Surface	27,220	0.4	8,064	2.4

Table 1. *(continued)*

Station	Latitude (°N)	Longitude (°W)	SCM Depth (m)	Euphotic Depth (m)	Sample	*Phaeocystis* spp. (cell L^{-1})	*Phaeocystis* spp. (µg C L^{-1})	Diatoms (cell L^{-1})	Diatoms (µg C L^{-1})
					SCM	6,637,000	94.2	30,740	10.3
G703	69.500	58.724	35	52	Surface	19,400	0.3	18,400	10.5
					SCM	64,770	0.9	10,590	1.3
G707	69.512	59.805	35	32.5	Surface	336,200	4.8	185,000	25.3
					SCM	1,260,000	17.9	39,310	2.6
G713	69.501	61.582	20	30.5	Surface	243,900	3.5	13,610	1.6
					SCM	859,100	12.2	7,812	0.4
G719	69.501	63.233	21	26	Surface	57,960	0.8	27,220	5.7
					SCM	181,400	2.6	105,800	9.5

[a]Not available.

of station G300 where bSi concentration and aggregate abundance remained high (0.66 µM and $>2 \times 10^3$ aggregates m^{-3}) 26 days after ice melting (**Figure 5**).

In **Figure 5**, the 7 stations with elevated aggregate abundances (G204, G207, G300, G309, G507, G512, and G707) plot above the other stations. Five of them were located at the ice edge (except G204 and G707), and all of them were located at sites with more than 0.6 µM of bSi. At these 7 stations, *Phaeocystis* spp. concentrations ranged from 8 to 74×10^5 cell L^{-1}, and diatom concentrations varied between 2 and 6×10^5 cell L^{-1}, except at station G300 where the diatom concentration was only 3.7×10^4 cell L^{-1} at the maximum aggregate concentration (at 55-m depth). At these high-aggregate stations, diatom communities were dominated by centric species (60%–92%) and specifically by *Chaetoceros* spp. and numerous *Thalassiosira* spp. Station G512 differed somewhat as pennate and centric species dominated the community equally. At this station, while *Chaetoceros* spp. were well represented, ice algal genera such as *Melosira*, *Cylindrotheca*, and *Entomoneis* were more abundant. Interestingly, at stations at the ice edge where aggregate abundance remained low at the surface (e.g., stations G605, G713, and G719), the concentrations of both *Phaeocystis* spp. and diatoms were one order of magnitude lower and the diatom community consisted mainly of pennate diatoms (87%–98%).

Pigment concentrations

Mean chlorophyll *a* concentration in the EML ranged from 0.06 to 3.28 µg L^{-1} across all stations, while mean EML phaeopigment concentration ranged from 0 to 0.1 µg L^{-1} (Table S2; Green Edge Database, 2021). Locations of the surface chlorophyll *a* maximum generally coincided with the surface bSi concentration maximum. We observed a gradient in phaeopigment concentrations from West to East, with maximum values at stations G3000 and G300 within the EML. Globally we observed a positive gradient of phaeopigments from ice-covered stations (negative OWD) to open water stations (positive OWD; **Figure 6**).

Distribution of copepod abundance

Under the ice (OWD < 0), the highest copepod abundances (>500 ind m$^-$) were observed above the EML, with maximum values deepening progressively as OWD increased (**Figure 7**).

PCA

Results of the PCA (**Figure 8**) indicated that the stations and parameters examined fell into three groups. The first group, comprised of pre-phytoplankton bloom stations, was characterized by high nutrient concentrations, SIC close to 1, low bSi and chlorophyll *a* concentrations, and low aggregate abundance. The second group of phytoplankton bloom stations was characterized by high bSi and chlorophyll *a* concentrations, with both *Phaeocystis* spp. and diatoms contributing to the phytoplankton community in the EML. The third group, called the post-phytoplankton bloom stations, was where we observed high phaeopigment concentrations in the EML and high OWD.

Discussion

Aggregation is an important process driving both vertical carbon export, through the formation of rapidly sinking particles (Turner, 2015), and carbon transfer to higher trophic levels (Leu et al., 2011; Wassmann et al., 2011; Leu et al., 2015; Forest et al., 2018). As such, aggregation represents the termination and the fate of phytoplankton blooms. The aggregation process and following massive sinking may be occasional and very fast (Alldredge and Gotschalk, 1989; Kiørboe et al., 1996; Prairie et al., 2019), and thus hard to observe and to predict. During the Green Edge campaign, we took advantage of the huge amount of data collected to try to identify what triggers aggregation of the spring phytoplankton bloom.

As not all phytoplankton species have the same ability to aggregate, we investigated the role played by the phytoplankton assemblage. According to the classical phytoplankton succession, *Phaeocystis* spp. blooms often follow diatom blooms, thriving when silicate concentrations drop below 2 µM (Smith et al., 1991; Smith, 1994; Smetacek,
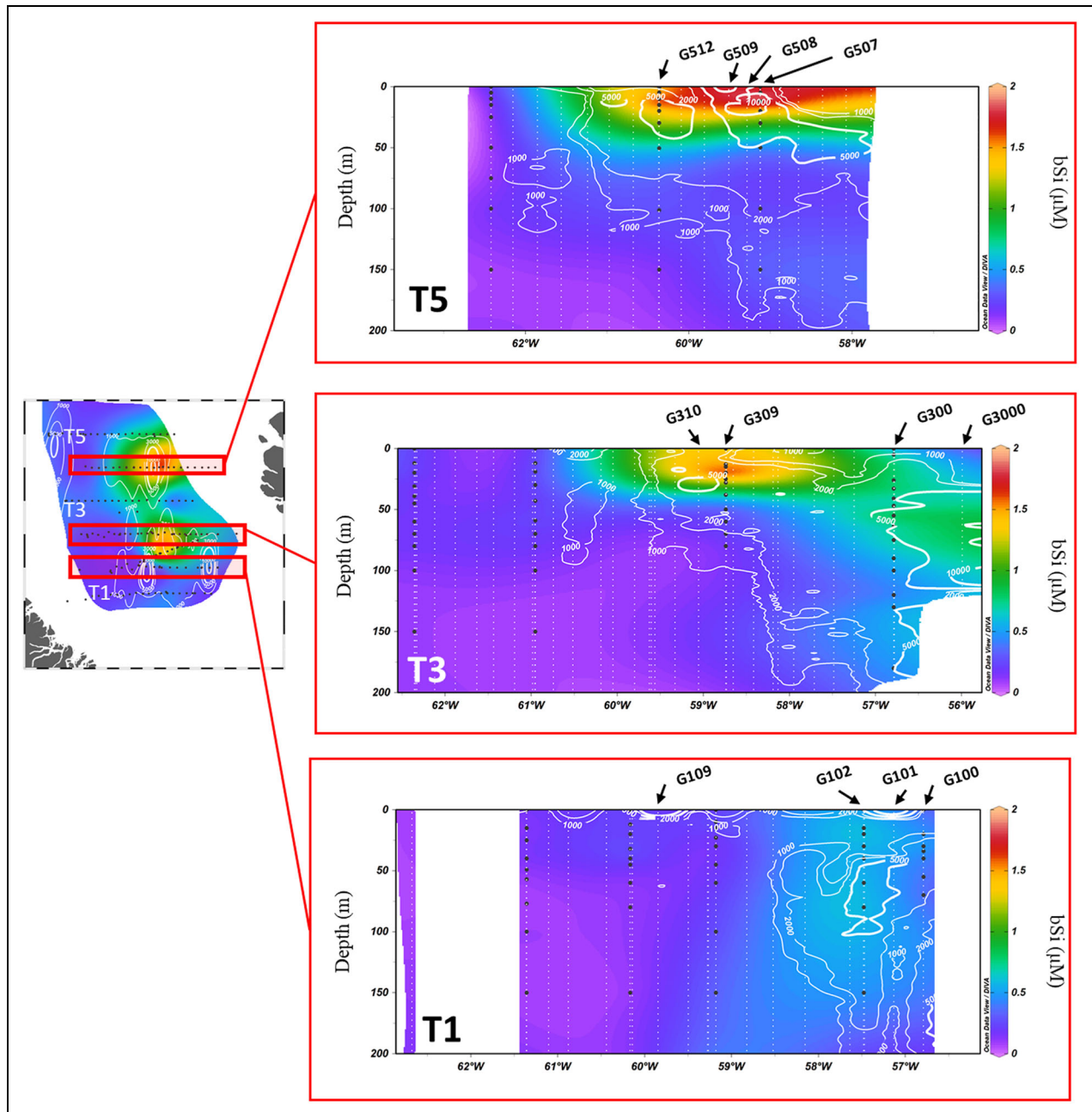
Figure 4. Vertical profiles of bSi concentration (μM, color-coded) along transects T5, T3, and T1. The white contour lines correspond to aggregate abundance (agg m^{-3}). Black dots correspond to discrete bSi samples; white dotted lines, to Underwater Video Profiler 5 profiles. Black arrows indicate stations of interest. DOI: https://doi.org/10.1525/elementa.2021.00001.f4

1999; Wassmann et al., 1999; Reigstad and Wassmann, 2007). Our results, however, demonstrated the co-occurrence of *Phaeocystis* spp. and diatoms throughout the sampling period. The occurrence of *Phaeocystis* spp. blooms is expected to increase with climate change (Marchant and Thomsen, 1994; Gabric et al., 2003; Schoemann et al., 2005), and the co-occurrence of both diatoms and *Phaeocystis* spp. is becoming increasingly common (Dybwad et al., 2021). Moreover, in the eastern central Arctic Basin, *Phaeocystis* spp. grow at high silicate concentrations (>2 μM; Smetacek, 1999; Wassmann et al., 1999; Gieskes et al., 2007; Degerlund and Eilertsen, 2010). Both diatoms and *Phaeocystis* spp. are generally associated with

strong aggregation events (Riebesell, 1993; Wassmann et al., 1999). The distribution patterns of diatoms and *Phaeocystis* spp. in our study globally matched the aggregate distribution observed along the sampling transects; however, the analysis in **Figure 5** revealed that the maximum aggregate concentrations correspond to maximum bSi concentrations, which are attributed to diatom biomass. More specifically, our results revealed maximum aggregate abundance at the surface when centric diatoms, mainly *Chaetoceros* spp., dominated the diatom community compared to stations dominated by pennate diatoms.

Many studies have shown that aggregation occurs more often during the late stage of the phytoplankton bloom, as

stickiness generally increases when senescent phytoplankton produce sticky organic compounds such as extracellular polysaccharide substances (EPS), Coomassie stainable particles, and transparent exopolymeric particles (TEP; Passow et al., 1994; Waite et al., 1995; Passow, 2000, 2002; Cisternas-Novoa et al., 2015; Cisternas-Novoa et al., 2019a; Cisternas-Novoa et al., 2019b).
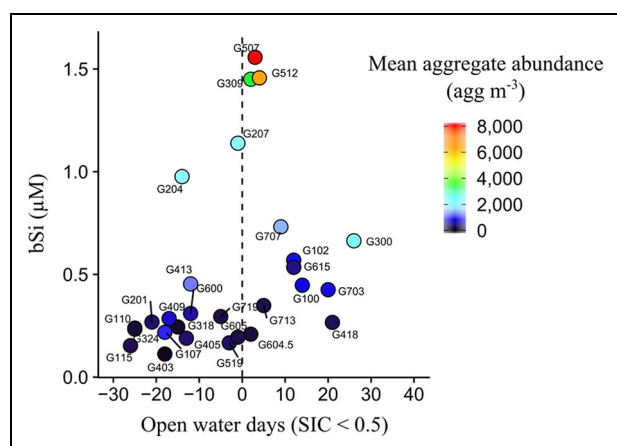

Figure 5. Mean biogenic silica concentration and aggregate abundance by open water days. Mean biogenic silica (bSi) concentrations (µM) are from the equivalent mixed layer (EML, 30-m depth) for 28 hydrological stations. Open water days correspond to number of days since the site became ice-free (positive values) or before the ice melt (negative values), where ice-free is defined as sea ice concentration below 50% (SIC < 0.5). Station data (solid circles) are color-coded for aggregate concentration (agg m^{-3}) in the EML. DOI: https://doi.org/10.1525/elementa.2021.00001.f5

Sea ice cover loss and nutrient limitation

In the Arctic, development of the phytoplankton bloom is strongly controlled by the ice cover and its melting. The senescence of phytoplankton blooms usually starts as nutrients become limiting and may be revealed by a change in pigment composition (Henriksen et al., 2002; Lewis et al., 2019). Nutrient limitation as discussed by Moore et al. (2013) may take the form of (1) a phytoplankton biomass threshold due to growth rate being limited by low nutrient concentrations (Blackman and Liebing theory); (2) physiological stress and deficiency of one element, for example, when the N:P or Si:N stoichiometric ratio is unbalanced and nitrogen becomes limiting, although the relationship between growth rate and stress due to nitrogen limitation can vary, and "the most deficient nutrient will not become limiting if all remain replete" (Moore et al., 2013); or (3) co-limitation, when two or more elements have been drawn down simultaneously to below the physiological level that allows for phytoplankton growth. Regarding values of half-saturation constants for nutrient uptake, the global average K_s for diatoms has been reported as 3.9 ± 5.0 µM ($n = 25$) for silicon, 1.6 ± 1.9 µM ($n = 35$) for nitrogen, and 0.24 ± 0.29 µM ($n = 14$) for phosphorus (Sarthou et al., 2005). For Arctic planktonic ecosystems, K_s is lower than 2 µM for silicate (1.15 µM from model parameters used in Zhang et al., 2010; 2 µM from in situ measurements in Krause et al., 2018) or even lower (e.g., 0.5 µM for nitrate and silicate for the Barents Sea; Slagstad and Støle-Hansen, 1991). From the K_s perspective, silicate concentrations under 2 µM and/or nitrate concentrations under 1.5 µM may be expected to limit diatom growth. Assuming these K_s values pertained to most of our stations, nitrate started to be limiting 2–10 days after ice melting, and silicate, 2 days before the ice melt (**Figure 3**). The stations with the highest aggregate abundance in the EML
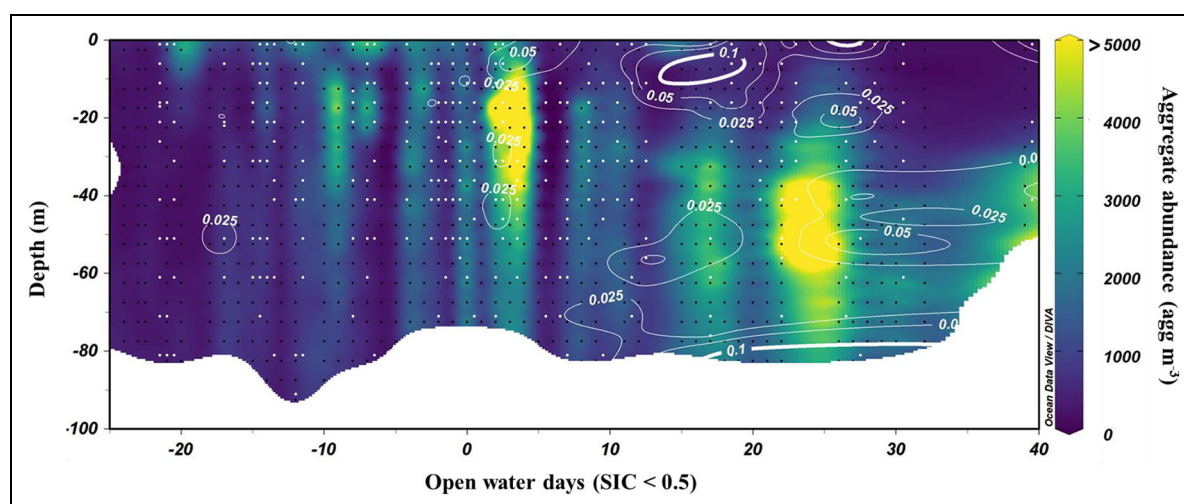

Figure 6. Vertical profiles of aggregate abundance and phaeopigment concentration by open water days. Aggregate abundance (agg m^{-3}), pooled from 137 hydrological stations, is indicated by color-coding. Open water days correspond to number of days since the site became ice-free (positive values) or before the ice melt (negative values), where ice-free is defined as sea ice concentration below 50% (SIC < 0.5). White contour lines correspond to phaeopigment concentrations (µg L^{-1}) measured from 52 hydrological stations; white dots, to discrete pigment samples. Black dots correspond to Underwater Video Profiler 5 profiles. DOI: https://doi.org/10.1525/elementa.2021.00001.f6
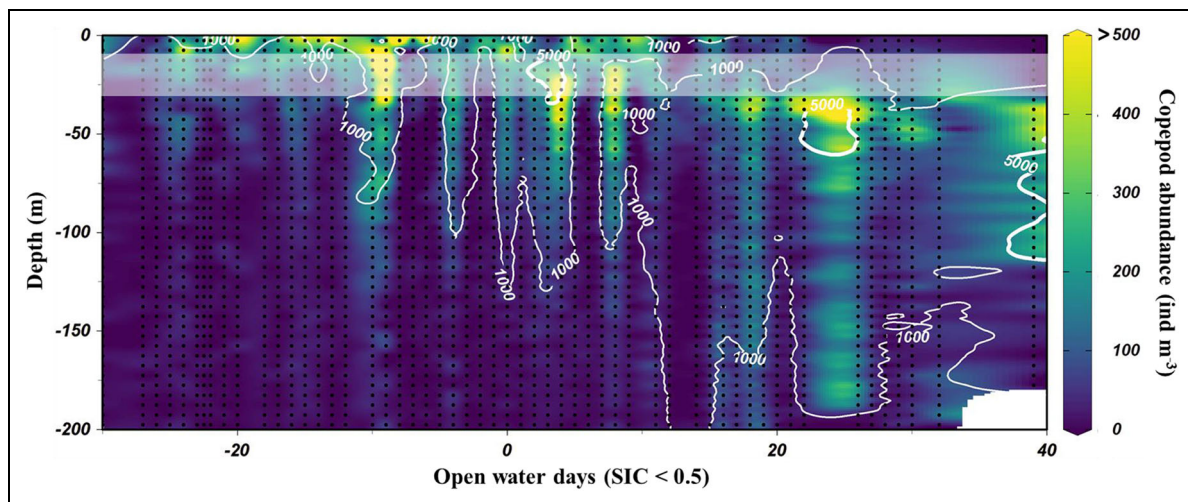
Figure 7. Vertical profiles of copepod abundance and aggregate abundance (agg m^{-3}, white contour line) by open water days. Copepod abundance (ind m^{-3}), pooled from 137 hydrological stations, is indicated by color-coding. Open water days correspond to number of days since the site became ice-free (positive values) or before the ice melt (negative values), where ice-free is defined as sea ice concentration below 50% (SIC < 0.5). The white contour lines correspond to aggregate concentrations (agg m^{-3}) measured from 137 hydrological stations. The horizontal shaded area represents the upper and lower depths of the equivalent mixing layer estimated by Randelhoff et al. (2019) during the *Amundsen* cruise. Black dots correspond to Underwater Video Profiler 5 profiles. DOI: https://doi.org/10.1525/elementa.2021.00001.f7

all had nitrate concentrations higher than the assumed K_s for nitrate (about 0.5–4.5 μM), but all had silicate concentrations around the value of the K_s measured for silicate in the Arctic by Krause et al. (2018; about 2 μM, **Figure 3**). Both nitrogen and silicon limitations could trigger aggregate formation in the EML, as they increase the mucus production that enhances stickiness (e.g., EPS, TEP; Passow et al., 1994; Waite et al., 1995; Passow, 2000, 2002; Cisternas-Novoa et al., 2015; Cisternas-Novoa et al., 2019a; Cisternas-Novoa et al., 2019b). As in Aumack and Juhl (2015), silicon limitation as defined by K_s values better explains high aggregate abundance in the EML than nitrate limitation in our study.

Phytoplankton bloom decline
A senescing phytoplankton bloom may be characterized by high phaeopigment concentrations (Tremblay et al., 1989; Riebesell, 1991; Barlow et al., 1993). However, in our data set, chlorophyll *a* was not degraded and phaeopigments were not concentrated at the ice edge. Hence, aggregates occurred when phytoplankton were still viable. Considering K_s values, aggregates appear to have formed when diatoms became limited by silicate, suggesting that nutrient limitation plays a major role in aggregation (Kaltenbock and Herndl, 1992; Magaletti et al., 2004; Beauvais et al., 2006; Aumack and Juhl, 2015). Other signals of stress were reported by Amiraux et al. (2017) during this same field campaign, including evidence for salinity stress of the bacterial communities in sea ice before it had completely melted and photo-oxidative stress of pelagic algae after the ice had melted. These authors suggested that EPS might protect the algae and their associated bacterial communities against abiotic stresses, as EPS production may be enhanced at these points.

In the PCA, which summarizes both the chemical and biological variables implicated in causing differences between stations (**Figure 8**), low phytoplankton growth (pre-phytoplankton bloom stations) was not associated with cell aggregation. As presented in **Figure 3**, the decrease in all nutrient concentrations in the EML (nitrate, silicate, and phosphate) appeared to correlate with the increase in OWD, which corresponds to the progressive utilization of nutrients as the phytoplankton bloom developed. At the phytoplankton bloom stations, the PCA shows a strong covariance between bSi concentration and aggregate abundance in the EML (red arrows in **Figure 8**), suggesting that nutrient-limited diatoms may be more efficient at aggregating in this ecosystem than *Phaeocystis* spp. even if their respective biomasses were not discriminated in the PCA (**Figure 8**). At the postbloom stations, high values of integrated aggregate abundance and depth of maximum aggregate abundance are congruent with phaeopigment concentration in the EML and depth of the maximum copepod abundance. Phaeopigment concentrations in the EML could be associated with a declining phytoplankton bloom and altered pigments (Tremblay et al., 1989; Riebesell, 1991; Barlow et al., 1993).

Copepod distribution
In Arctic environments, zooplankton communities are dominated by only a few copepod species. Only *C. glacialis* and *C. finmarchicus* adults were counted in the eastern, Atlantic-influenced part of the Bay where they appeared in slightly higher numbers. *C. hyperboreus, M. longa*, and *Pseudocalanus* spp. adults were spread homogeneously among the stations (Vilgrain et al., 2021, on the same cruise). As the maximum aggregate abundance deepened
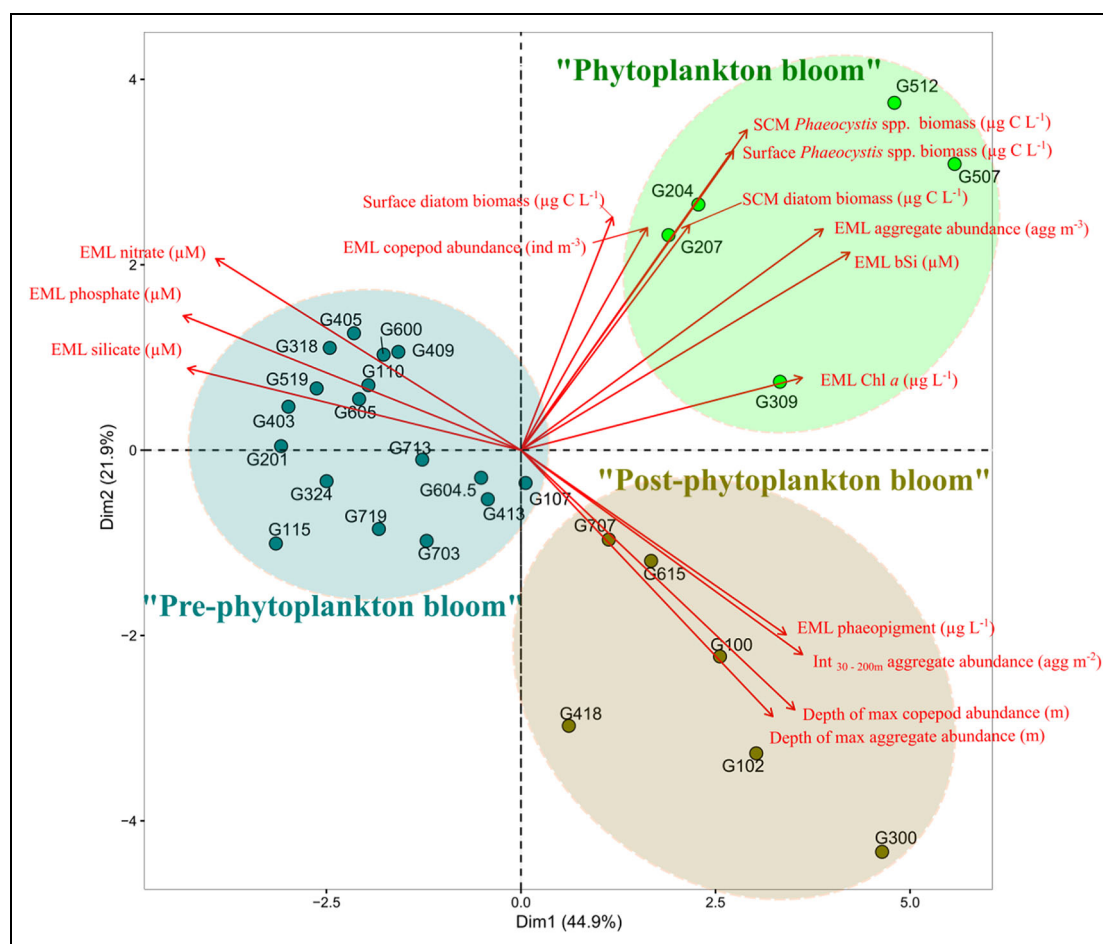
Figure 8. Principal component analysis of stations and parameters sampled during the *Amundsen* cruise. Solid circles indicate the 28 stations sampled, color-coded by group (the 3 shaded areas); red arrows represent the explanatory variables. The first dimension (*x*-axis) represents 44.9% of the variance. The second dimension (*y*-axis) represents 21.9% of the variance. EML indicates equivalent mixing layer as presented in Randelhoff et al. (2019). DOI: https://doi.org/10.1525/elementa.2021.00001.f8

with OWD, the same pattern was seen with depth of the maximum copepod abundance (**Figure 2**). When phytoplankton in the surface began to degrade, as evidenced by higher phaeopigment concentrations (Sanmartin et al., 2011), copepods seemed to migrate below the EML following the aggregates. As diatom cells can stay viable for long periods inside aggregates (Garvey et al., 2007, Agustí et al., 2015), sinking aggregates may be a better food source for copepods than degraded phytoplankton cells in surface waters (Helling and Baars, 1985; Barlow et al., 1993). In the post-phytoplankton bloom conditions, copepods seemed to forage deeper for food and switch their feeding behavior, as suggested in other studies (Dagg, 1993; Lampitt et al., 1993; Steinberg, 1995; Dilling et al., 1998; Kiørboe, 2000; Dilling and Brzezinski, 2004; Koski et al., 2017; Toullec et al., 2019). Copepods are the dominant component of the zooplankton communities that may actively participate in particle dynamics by breaking apart aggregates, as previously suggested from laboratory experiments (Toullec et al., 2019), mesocosm experiments (Moriceau et al., 2018; Taucher et al., 2018), and in situ studies (Dilling and Alldredge, 2000), or by

favoring the aggregation process of free phytoplankton cells (Taucher et al., 2018; Toullec et al., 2019). At the ice edge, maximum copepod and aggregate abundances were found at similarly shallow depths; however, copepods were much less numerous than aggregates (1:1,000 to 1:100), and the average aggregate size was not affected by fragmentation due to copepod feeding activities. Further from the ice edge, the maximum copepod and aggregate abundances were deeper but again at similar depths. Although copepods may have gone deeper to escape predation from fishes and seabirds (Lampert, 1989; Fortier et al., 2001; Karnovsky et al., 2003; Schmid and Fortier, 2019), they may have also descended to feed on phytoplankton aggregates (Bochdansky and Herndl, 1992; Bochdansky et al., 1995; Green and Dagg, 1997; Shanks and Walters, 1997; Goldthwait et al., 2004; Koski et al., 2017; Toullec et al., 2019). Low food quality, illustrated by high phaeopigment concentrations, in the surface at stations where both aggregate and copepod maxima were deep suggests that copepods were following the aggregates to feed on them because they contained less degraded algal cells (Garvey et al., 2007).

Conclusions

The purpose of this study was to consider the importance of hydrobiological dynamics on the formation and distribution of macroaggregates (marine snow) in Baffin Bay during spring 2016. Here, we combined hydrological parameters and advanced optical particle analysis (UVP5 deployment and particle quality based on automatic determination) to describe the distribution and fate of the aggregates in an Arctic ecosystem.

Ice melting drives the hydrological context, and thus the phytoplankton phenology in Baffin Bay. Contrary to previous expectations of bloom succession, we observed the simultaneous occurrence of diatoms and *Phaeocystis* spp. blooming at the ice edge. Climate change has been identified as responsible for this phenological pattern, which is expected to become increasingly common (Marchant and Thomsen, 1994; Gabric et al., 2003; Schoemann et al., 2005). Indeed, the hydrodynamic context would be affected by climate change mainly by a reduction in the EML, leading to a decrease in the vertical input of nutrients (Tremblay et al., 2002; 2015), an inflow modification that will tend to increase nutrient limitation in Baffin Bay. During this study in Baffin Bay, diatoms still dominated phytoplankton groups during the spring bloom, with their aggregation beginning once silicate concentrations dropped to 2 μM, close to the physiologically limiting value at this latitude. However, nitrate is the first limiting nutrient in the Arctic and was observed to be limiting later in our study. Aggregation may be triggered by the first nutrient that reaches a limiting concentration that stresses the diatoms, suggesting that aggregation may be enhanced by increased stratification, regardless of the nutrient involved. Haline stress resulting from ice melting possibly also contributes to the aggregation process. If primary production increases in open waters in this region, as hypothesized in the context of climate change (Babin, 2020; Lewis et al., 2020), our study suggests a concomitant increase in aggregate formation and thus a high potential for increased vertical export through the gravity pathway. As copepods go deeper, switching their feeding target from free phytoplankton cells to sinking aggregates, the active transport of matter due to zooplankton migration may also increase.

Data accessibility statement

All data are accessible at the Green Edge Database (2021), available at http://www.obs-vlfr.fr/proof/php/GREENEDGE/greenedge.php, and will be made public prior to publication.

Supplemental files

The supplemental files for this article can be found as follows:

Table S1. List of parameters per sampling stations.
Table S2. Pigment concentrations in the EML.

Acknowledgments

The project is conducted under the scientific coordination of the Canada Excellence Research Chair on remote sensing of Canada's new Arctic frontier and the CNRS and Université Laval Takuvik Joint International Laboratory (UMI3376). We thank officers and crew of CCGS *Amundsen*, Marie-Hélène Forget, and Joannie Ferland for organizing the fieldwork and all other scientists and technicians involved in the Green Edge campaign for their contributions to fieldwork and data collection. We also thank the reviewers and editors who brought considerable improvements to the article.

Competing interests

The authors have no competing interests to declare.

Author contributions

Contributed to conception and design: JT, BM.

Contributed to acquisition of data: JT, BM, MB.

Contributed to analysis and interpretation of data: JT, BM, DV.

Drafted and/or revised the article: JT, BM, LG, DV, AL, MB.

Approved the submitted version for publication: JT, BM, DV, LG, AL, MB.

References

Agustí, S, González-Gordillo, JI, Vaqué, D, Estrada, M, Cerezo, MI, Salazar, G, Gasol, JM, Duarte, CM. 2015. Ubiquitous healthy diatoms in the deep sea confirm deep carbon injection by the biological pump. *Nature Communications* **6**: 1–8.

Alldredge, AL, Gotschalk, C. 1989. Direct observations of the mass flocculation of diatom blooms: Characteristics, settling velocities and formation of diatom aggregates. *Deep Sea Research Part A: Oceanographic Research Papers* **36**(2): 159–171. DOI: http://dx.doi.org/10.1016/0198-0149(89)90131-3.

Amiraux, R, Belt, ST, Vaultier, F, Galindo, V, Gosselin, M, Bonin, P, Rontani, J-F. 2017. Monitoring photo-oxidative and salinity-induced bacterial stress in the Canadian Arctic using specific lipid tracers. *Marine Chemistry* **194**: 89–99.

Arrigo, KR. 2014. Sea ice ecosystems. *Annual Review of Marine Science* **6**: 439–467.

Arrigo, KR, van Dijken, GL. 2011. Secular trends in Arctic Ocean net primary production. *Journal of Geophysical Research: Oceans* **116**(C9). DOI: http://dx.doi.org/10.1029/2011JC007151.

Assmy, P, Fernández-Méndez, M, Duarte, P, Meyer, A, Randelhoff, A, Mundy, C, Olsen, LM, Kauko, HM, Bailey, A, Chierici, M, Cohen, L, Doulgeris, A, Ehn, J, Fransson, A, Gerland, S, Hop, H, Hudson, S, Hughes, N, Itkin, P, Johnsen, G, King, J, Koch,

B, Koenig, Z, Kwaśniewski, S, Laney, S, Nicolaus, M, Pavlov, A, Polashenski, C, Provost, C, Rösel, A, Sandbu, M, Spreen, G, Smedsrud, L, Sundfjord, A, Taskjelle, T, Tatarek, A, Wiktor, J, Wagner, P, Wold, A, Steen, H, Granskog, M. 2017. Leads in Arctic pack ice enable early phytoplankton blooms below snow-covered sea ice. *Scientific Reports* **7**(1). DOI: http://dx.doi.org/10.1038/srep40850.

Aumack, CF, Juhl, AR. 2015. Light and nutrient effects on the settling characteristics of the sea ice diatom *Nitzschia frigida*. *Limnology and Oceanography* **60**(3): 765–776. DOI: http://dx.doi.org/https://doi.org/10.1002/lno.10054.

Babin, M. 2020. Climate change tweaks Arctic marine ecosystems. *Science* **369**(6500): 137–138.

Barlow, RG, Mantoura, RFC, Gough, MA, Fileman, TW. 1993. Phaeopigment distribution during the 1990 spring bloom in the northeastern Atlantic. *Deep Sea Research Part I: Oceanographic Research Papers* **40**(11–12): 2229–2242.

Beauvais, S, Pedrotti, M L, Egge, J, Iversen, K, Marrasé, C. 2006. Effects of turbulence on TEP dynamics under contrasting nutrient conditions: Implications for aggregation and sedimentation processes. *Marine Ecology Progress Series* **323**: 47–57.

Beitsch, A, Kaleschke, L, Kern, S. 2014. Investigating high-resolution AMSR2 sea ice concentrations during the February 2013 fracture event in the Beaufort Sea. *Remote Sensing* **6**(5): 3841–3856. DOI: http://doi.org/10.3390/rs6053841.

Bochdansky, AB, Herndl, GJ. 1992. Ecology of amorphous aggregations (marine snow) in the Northern Adriatic Sea. 111. Zooplankton interactions with marine snow. *Marine Ecology Progress Series* 87: 135–146.

Bochdansky, AB, Puskaric, S, Herndl, GJ. 1995. Influence of zooplankton grazing on free dissolved enzymes in the sea. *Marine Ecology Progress Series* **121**: 53–63.

Cavan, EL, Laurenceau-Cornec, EC, Bressac, M, Boyd, PW. 2019. Exploring the ecology of the mesopelagic biological pump. *Progress in Oceanography* **176**: 102125.

Cisternas-Novoa, C, Le Moigne, FAC, Engel, A. 2019a. Composition and vertical flux of particulate organic matter to the oxygen minimum zone of the central Baltic Sea: Impact of a sporadic North Sea inflow. *Biogeosciences* **16**(4): 927–947. DOI: http://dx.doi.org/https://doi.org/10.5194/bg-16-927-2019.

Cisternas-Novoa, C, Lee, C, Engel, A. 2015. Transparent exopolymer particles (TEP) and Coomassie stainable particles (CSP): Differences between their origin and vertical distributions in the ocean. *Marine Chemistry* **175**: 56–71. DOI: http://dx.doi.org/10.1016/j.marchem.2015.03.009.

Cisternas-Novoa, C, Lee, C, Tang, T, de Jesus, R, Engel, A. 2019b. Effects of higher CO_2 and temperature on exopolymer particle content and physical properties of marine aggregates. *Frontiers in Marine Science* **5**: 500.

Coachman, LK, Aagaard, K. 1974. Physical oceanography of Arctic and subarctic seas, in Herman, Y ed., *Marine geology and oceanography of the Arctic seas*. New York, NY: Springer: 1–72.

Comiso, JC. 2002. A rapidly declining perennial sea ice cover in the Arctic. *Geophysical Research Letters* **29**(20): 17-1–17-4.

Comiso, JC, Parkinson, CL, Gersten, R, Stock, L. 2008. Accelerated decline in the Arctic sea ice cover. *Geophysical Research Letters* **35**(1). DOI: http://dx.doi.org/10.1029/2007GL031972.

Dagg, MJ. 1993. Sinking particles as a possible source of nutrition for the large calanoid copepod *Neocalanus cristatus* in the subarctic Pacific Ocean. *Deep Sea Research Part I: Oceanographic Research Papers* **40**(7): 1431–1445. DOI: http://dx.doi.org/10.1016/0967-0637(93)90121-I.

Darnis, G, Barber, DG, Fortier, L. 2008. Sea ice and the onshore–offshore gradient in pre-winter zooplankton assemblages in southeastern Beaufort Sea. *Journal of Marine Systems* **74**(3–4): 994–1011.

Darnis, G, Hobbs, L, Geoffroy, M, Grenvald, JC, Renaud, PE, Berge, J, Cottier, F, Kristiansen, S, Daase, M, Søreide, JE, Wold, A, Morata, N, Gabrielse, T. 2017. From polar night to midnight sun: Diel vertical migration, metabolism and biogeochemical role of zooplankton in a high Arctic fjord (Kongsfjorden, Svalbard). *Limnology and Oceanography* **62**(4): 1586–1605. DOI: http://dx.doi.org/10.1002/lno.10519.

Darnis, G, Robert, D, Pomerleau, C, Link, H, Archambault, P, Nelson, RJ, Geoffroy, M, Tremblay, J-É, Lovejoy, C, Ferguson, SH, Hunt, BPV, Fortier, L. 2012. Current state and trends in Canadian Arctic marine ecosystems: II. Heterotrophic food web, pelagic-benthic coupling, and biodiversity. *Climatic Change* **115**(1): 179–205. DOI: http://dx.doi.org/10.1007/s10584-012-0483-8.

Degerlund, M, Eilertsen, HC. 2010. Main species characteristics of phytoplankton spring blooms in NE Atlantic and Arctic waters (68–80°N). *Estuaries and Coasts* **33**(2): 242–269. DOI: http://dx.doi.org/10.1007/s12237-009-9167-7.

Dilling, L, Alldredge, AL. 2000. Fragmentation of marine snow by swimming macrozooplankton: A new process impacting carbon cycling in the sea. *Deep Sea Research Part I: Oceanographic Research Papers* **47**(7): 1227–1245.

Dilling, L, Brzezinski, MA. 2004. Quantifying marine snow as a food choice for zooplankton using stable silicon isotope tracers. *Journal of Plankton Research* **26**(9): 1105–1114. DOI: http://dx.doi.org/10.1093/plankt/fbh103.

Dilling, L, Wilson J, Steinberg, D, Alldredge, A. 1998. Feeding by the euphausiid *Euphausia pacifica* and the copepod *Calanus pacificus* on marine snow. *Marine Ecology Progress Series* **170**: 189–201.

Dybwad, C, Assmy, P, Olsen, LM, Peeken, I, Nikolopoulos, A, Krumpen, T, Randelhoff, A, Tatarek, A, Wiktor, JM, Reigstad, M. 2021. Carbon export in

the seasonal sea ice zone north of Svalbard from winter to late summer. *Frontiers in Marine Science* **7**: 525800. DOI: http://dx.doi.org/10.3389/fmars. 2020.525800.

Feng, Z, Ji R, Campbell, RG, Ashjian, CJ, Zhang, J. 2016. Early ice retreat and ocean warming may induce copepod biogeographic boundary shifts in the Arctic Ocean. *Journal of Geophysical Research: Oceans* **121**(8): 6137–6158.

Forest, A, Sampei, M, Makabe, R, Sasaki, H, Barber, DG, Gratton, Y, Wassmann, P, Fortier, L. 2018. The annual cycle of particulate organic carbon export in Franklin Bay (Canadian Arctic): Environmental control and food web implications. *Journal of Geophysical Research: Oceans* **113**. DOI: http://dx.doi.org/10.1029/2007JC004262@10.1002/(ISSN)2169-9291.CASES1.

Fortier, M, Fortier, L, Hattori, H, Saito, H, Legendre, L. 2001. Visual predators and the diel vertical migration of copepods under Arctic sea ice during the midnight sun. *Journal of Plankton Research* **23**(11): 1263–1278. DOI: http://dx.doi.org/10.1093/plankt/23.11.1263.

Gabric, AJ, Cropp, R, Hirst, T, Marchant, H. 2003. The sensitivity of dimethyl sulfide production to simulated climate change in the Eastern Antarctic Southern Ocean. *Tellus B* **55**(5): 966–981.

Garvey, M, Moriceau, B, Passow, U. 2007. Applicability of the FDA assay to determine the viability of marine phytoplankton under different environmental conditions. *Marine Ecology Progress Series* **352**: 17–26.

Gieskes, WWC, Leterme, SC, Peletier, H, Edwards, M, Reid, PC. 2007. *Phaeocystis* colony distribution in the North Atlantic Ocean since 1948, and interpretation of long-term changes in the *Phaeocystis* hotspot in the North Sea. *Biogeochemistry* **83**(1): 49–60.

Goldthwait, S, Yen, J, Brown, J, Alldredge, A. 2004. Quantification of marine snow fragmentation by swimming euphausiids. *Limnology and Oceanography* **49**(4): 940–952.

Gorsky, G, Ohman, MD, Picheral, M, Gasparini, S, Stemmann, L, Romagnan, J-B, Cawood, A, Pesant, S, García-Comas, C, Prejger F. 2010. Digital zooplankton image analysis using the ZooScan integrated system. *Journal of Plankton Research* **32**(3): 285–303. DOI: http://dx.doi.org/10.1093/plankt/fbp124.

Grasshoff, K, Kremling, K, Ehrhardt, M. 2009. *Methods of seawater analysis*. Hoboken, NJ: John Wiley.

Green Edge Database. 2021. Portal to LEFE CYBER Database for All Green Edge Project Data From 2015 to Present [dataset]. Available at http://www.obs-vlfr.fr/proof/php/GREENEDGE/greenedge.php.

Green, EP, Dagg, MJ. 1997. Mesozooplankton associations with medium to large marine snow aggregates in the northern Gulf of Mexico. *Journal of Plankton Research* **19**(4): 435–447. DOI: http://dx.doi.org/10.1093/plankt/19.4.435.

Hansen, B, Christiansen, S, Pedersen, G. 1996. Plankton dynamics in the marginal ice zone of the central Barents Sea during spring: Carbon flow and structure of the grazer food chain. *Polar Biology* **16**(2): 115–128. DOI: http://dx.doi.org/10.1007/BF02390432.

Helling, GR, Baars, MA. 1985. Changes of the concentrations of chlorophyll and phaeopigment in grazing experiments. *Hydrobiological Bulletin* **19**(1): 41–48.

Henriksen, P, Riemann, B, Kaas, H, Sørensen, HM, Sørensen, HL. 2002. Effects of nutrient-limitation and irradiance on marine phytoplankton pigments. *Journal of Plankton Research* **24**(9): 835–858.

Henson, S, Le Moigne, FAC, Giering, S. 2019. Drivers of carbon export efficiency in the global ocean. *Global Biogeochemical Cycles* **33**. DOI: http://dx.doi.org/10.1029/2018GB006158.

Hillebrand, H, Dürselen, CD, Kirschtel, D, Pollingher, U, Zohary, T. 1999. Biovolume calculation for pelagic and benthic microalgae. *Journal of Phycology* **35**(2): 403–424.

Janout, MA, Hölemann, J, Waite, AM, Krumpen, T, von Appen, W-J, Martynov, F. 2016. Sea-ice retreat controls timing of summer plankton blooms in the Eastern Arctic Ocean. *Geophysical Research Letters* **43**(24): 12,493–12,501. DOI: http://dx.doi.org/10.1002/2016GL071232.

Kaltenböck, E, Herndl, GJ. 1992. Ecology of amorphous aggregations (marine snow) in the Northern Adriatic Sea. IV. Dissolved nutrients and the autotrophic community associated with marine snow. *Marine Ecology Progress Series* **87**: 147–147.

Karnovsky, NJ, Kwaśniewski, S, Węslawski, JM, Walkusz, W, Beszczyńska-Möller, A. 2003. Foraging behavior of little auks in a heterogeneous environment. *Marine Ecology Progress Series* **253**: 289–303.

Kellogg, CTE, Carpenter, SD, Renfro, AA, Sallon, A, Michel, C, Cochran, JK, Deming, JW. 2011. Evidence for microbial attenuation of particle flux in the Amundsen Gulf and Beaufort Sea: Elevated hydrolytic enzyme activity on sinking aggregates. *Polar Biology* **34**(12): 2007–2023. DOI: http://dx.doi.org/10.1007/s00300-011-1015-0.

Kiørboe, T. 2000. Colonization of marine snow aggregates by invertebrate zooplankton: Abundance, scaling, and possible role. *Limnology and Oceanography* **45**(2): 479–484.

Kiørboe, T, Saiz, E, Viitasalo, M. 1996. Prey switching behaviour in the planktonic copepod Acartia tonsa. *Marine Ecology Progress Series* **143**: 65–75. DOI: http://dx.doi.org/10.3354/meps143065.

Koski, M, Boutorh, J, de la Rocha, C. 2017. Feeding on dispersed vs. aggregated particles: The effect of zooplankton feeding behavior on vertical flux. *PLoS One* **12**(5): e0177958. DOI: http://dx.doi.org/10.1371/journal.pone.0177958.

Krause, JW, Duarte, CM, Marquez, IA, Assmy, P, Fernández-Méndez, M, Wiedmann, I, Wassmann, P, Kristiansen, S, Agustí, S. 2018. Biogenic silica

production and diatom dynamics in the Svalbard region during spring. *Biogeosciences* **15**(21): 6503–6517.

Kwok, R, Rothrock, DA. 2009. Decline in Arctic sea ice thickness from submarine and ICESat records: 1958–2008. *Geophysical Research Letters* **36**: L15501.

Lafond, A, Leblanc, K, Queguiner, B, Moriceau, B, Leynaert, A, Cornet, V, Legras, J, Ras, J, Parenteau, M, Garcia, N, Babin, M, Tremblay, J-É. 2019. Late spring bloom development of pelagic diatoms in Baffin Bay. *Elementa: Science of the Anthropocene* **7**. DOI: http://dx.doi.org/10.1525/elementa.382.

Lampert, W. 1989. The adaptive significance of diel vertical migration of zooplankton. *Functional Ecology* **3**(1): 21–27.

Lampitt, RS, Wishner, KF, Turley, CM, Angel, MV. 1993. Marine snow studies in the Northeast Atlantic Ocean: Distribution, composition and role as a food source for migrating plankton. *Marine Biology* **116**(4): 689–702.

Legendre, P, Legendre, L. 2012. *Numerical ecology.* 3rd ed. Amsterdam, the Netherlands: Elsevier Science.

Leiknes, Ø, Etter, S A, Tokle, N E, Bergvik, M, Vadstein, O, Olsen, Y. 2016. The effect of essential fatty acids for the somatic growth in nauplii of *Calanus finmarchicus*. *Frontiers in Marine Science* **3**: 33.

Leu, E, Mundy, CJ, Assmy, P, Campbell, K, Gabrielsen, T, Gosselin, M, Juul-Pedersen, T, Gradinger, R. 2015. Arctic spring awakening—Steering principles behind the phenology of vernal ice algal blooms. *Progress in Oceanography* **139**: 151–170. DOI: http://dx.doi.org/10.1016/j.pocean.2015.07.012.

Leu, E, Søreide, JE, Hessen, DO, Falk-Petersen, S, Berge, J. 2011. Consequences of changing sea-ice cover for primary and secondary producers in the European Arctic shelf seas: timing, quantity, and quality. *Progress in Oceanography* **90**(1–4): 18–32.

Lewis, KM, Arntsen, AE, Coupel, P, Joy-Warren, H, Lowry, KE, Matsuoka, A, Mills, MM, van Dijken, GL, Arrigo, KR. 2019. Photoacclimation of Arctic Ocean phytoplankton to shifting light and nutrient limitation. *Limnology and Oceanography* **64**(1): 284–301.

Lewis, KM, van Dijken, GL, Arrigo, KR. 2020. Changes in phytoplankton concentration now drive increased Arctic Ocean primary production. *Science* **369**(6500): 198–202. DOI: http://dx.doi.org/10.1126/science.aay8380.

Magaletti, E, Urbani, R, Sist, P, Ferrari, CR, Cicero, AM. 2004. Abundance and chemical characterization of extracellular carbohydrates released by the marine diatom *Cylindrotheca fusiformis* under N-and P-limitation. *European Journal of Phycology* **39**(2): 133–142.

Marchant, HJ, Thomsen, HA. 1994. Haptophytes in polar waters. *Systematic Association Special Volume* **51**: 209–209.

Mari, X, Rassoulzadegan, F, Brussaard, CPD, Wassmann, P. 2005. Dynamics of transparent exopolymeric particles (TEP) production by *Phaeocystis globosa* under N- or P-limitation: A controlling factor of the retention/export balance. *Harmful Algae* **4**(5): 895–914. DOI: http://dx.doi.org/10.1016/j.hal.2004.12.014.

Massicotte, P, Amiraux, R, Amyot, M-P, Archambault, P, Ardyna, M, Arnaud, L, Artigue, L, Aubry, C, Ayotte, P, Bécu, G, Bélanger, S, Benner, R, Bittig, HC, Bricaud, A, Brossier, É, Bruyant, F, Chauvaud, L, Christiansen-Stowe, D, Claustre, H, Cornet-Barthaux, V, Coupel, P, Cox, C, Delaforge, A, Dezutter, T, Dimier, C, Dominé, F, Dufour, F, Dufresne, C, Dumont, D, Ehn, J, Else, B, Ferland, J, Forget, M-H, Fortier, L, Galí, M, Galindo, V, Gallinari, M, Garcia, N, Gérikas-Ribeiro, C, Gourdal, M, Gourvil, P, Goyens, C, Grondin, P-L, Guillot, P, Guilmette, C, Houssais, MN, Joux, F, Lacour, L, Lacour, T, Lafond, A, Lagunas, J, Lalande, C, Laliberté, J, Lambert-Girard, S, Larivière, J, Lavaud, J, Le Gall, F, LeBaron, A, Leblanc, K, Legras, J, Lemire, M, Levasseur, M, Leymarie, E, Leynaert, A, Lopes dos Santos, A, Lourenço, A, Mah, D, Marec, C, Marie, D, Martin, N, Marty, C, Marty, S, Massé, G, Matsuoka, A, Matthes, L, Moriceau, B, Muller, P-E, Mundy, CJ, Neukermans, G, Oziel, L, Panagiotopoulos, C, Pangazi, J-J, Picard, G, Picheral, M, Pinczon du Sel, F, Pogorzelec, N, Probert, I, Queguiner, B, Raimbault, P, Ras, J, Rehm, E, Reimer, E, Rontani, J-F, Rysgaard, S, Saint-Béat, B, Sampei, M, Sansoulet, J, Schmidt, S, Sempéré, R, Sévigny, C, Shen, Y, Tragin, M, Tremblay, J-É, Vaulot, D, Verin, G, Vivier, F, Vladoiu, A, Whitehead, J, Babin, M. 2019. Green Edge ice camp campaigns: Understanding the processes controlling the under-ice Arctic phytoplankton spring bloom. *Earth System Science Data Discussions* 1–42. DOI: http://dx.doi.org/10.5194/essd-2019-160.

Massicotte, P, Bécu, G, Lambert-Girard, S, Leymarie, E, Babin, M. 2018. Estimating underwater light regime under spatially heterogeneous sea ice in the Arctic. *Applied Sciences* **8**(12): 2693.

Masson-Delmotte, V, Zhai, P, Pörtner, H-O, Roberts, D, Skea, J, Shukla, PR, Pirani, A, Moufouma-Okia, W, Péan, C, Pidcock, R, Connors, S, Matthews, JBR, Chen, Y, Zhou, X, Gomis, MI, Lonnoy, E, Maycock, T, Tignor, M, Waterfield, T. 2018. *Global warming of 1.5°C. An IPCC special report on the impacts of global warming of 1.5°C above pre-industrial levels and related global greenhouse gas emission pathways, in the context of strengthening the global response to the threat of climate change, sustainable development, and efforts to eradicate poverty.* Geneva, Switzerland: Intergovernmental Panel on Climate Change (IPCC).

Moore, CM, Mills, MM, Arrigo, KR, Berman-Frank, I, Bopp L, Boyd, PW, Galbraith, ED, Geider, RJ, Guieu, C, Jaccard, SL, Jickells, TD, La Roche, J, Lenton, TM, Mahowald, NM, Marañón, E, Marinov, I, Moore, JK, Nakatsuka, T, Oschlies, A,

Saito, MA, Thingstad, TF, Tsuda, A, Ulloa, O. 2013. Processes and patterns of oceanic nutrient limitation. *Nature Geoscience* **6**(9): 701–710. DOI: http://dx.doi.org/10.1038/ngeo1765.

Moriceau, B, Gallinari, M, Soetaert, K, Ragueneau, O. 2007. Importance of particle formation to reconstructed water column biogenic silica fluxes: From particle dissolution rates to $BSiO_2$ fluxes. *Global Biogeochemical Cycles* **21**(3). DOI: http://dx.doi.org/10.1029/2006GB002814.

Moriceau, B, Iversen, MH, Gallinari, M, Evertsen, A-JO, Le Goff, M, Beker, B, Boutorh, J, Corvaisier, R, Coffineau, N, Donval, A, Giering, SLC, Koski, M, Lambert, C, Lampitt, RS, Le Mercier, A, Masson, A, Stibor, H, Stockenreiter, M, De La Rocha, CL. 2018. Copepods boost the production but reduce the carbon export efficiency by diatoms. *Frontiers in Marine Science* **5**. DOI: http://dx.doi.org/10.3389/fmars.2018.00082.

Nelson, DM, Smith, WO, Muench, RD, Gordon, LI, Sullivan, CW, Husby, DM. 1989. Particulate matter and nutrient distributions in the ice-edge zone of the Weddell Sea: Relationship to hydrography during late summer. *Deep Sea Research Part A: Oceanographic Research Papers* **36**(2): 191–209. DOI: http://dx.doi.org/10.1016/0198-0149(89)90133-7.

Newton, JL, Aagaard, K, Coachman, LK. 1974. Baroclinic eddies in the Arctic Ocean. *Deep Sea Research and Oceanographic Abstracts* **21**: 707–719.

Nielsen, TG, Hansen, B. 1995. Plankton community structure and carbon cycling on the western coast of Greenland during and after the sedimentation of a diatom bloom. *Marine Ecology Progress Series* **125**: 239–257. DOI: http://dx.doi.org/10.3354/meps125239.

Oziel, L, Massicotte, P, Randelhoff, A, Ferland, J, Vladoiu, A, Lacour, L, Galindo, V, Lambert-Girard, S, Dumont, D, Cuypers, Y, Bouruet-Aubertot, P, Galindo, V, Marec, C, Forget, M-H, Garcia, N, Raimbault, P, Houssais, MN, Babin, M. 2019. Environmental factors influencing the seasonal dynamics of spring algal blooms in and beneath sea ice in western Baffin Bay. *Elementa: Science of the Anthropocene* **7**(1): 34. DOI: http://dx.doi.org/10.1525/elementa.372.

Paasche, E. 1973. Silicon and the ecology of marine plankton diatoms. I. *Thalassiosira pseudonana* (*Cyclotella nana*) grown in a chemostat with silicate as limiting nutrient. *Marine Biology* **19**(2): 117–126. DOI: http://dx.doi.org/10.1007/BF00353582.

Passow, U. 2000. Formation of transparent exopolymer particles, TEP, from dissolved precursor material. *Marine Ecology Progress Series* **192**: 1–11.

Passow, U. 2002. Transparent exopolymer particles (TEP) in aquatic environments. *Progress in Oceanography* **55**(3): 287–333. DOI: http://dx.doi.org/10.1016/S0079-6611(02)00138-6.

Passow, U, Alldredge, AL, Logan, BE. 1994. The role of particulate carbohydrate exudates in the flocculation of diatom blooms. *Deep Sea Research Part I: Oceanographic Research Papers* **41**(2): 335–357. DOI: http://dx.doi.org/10.1016/0967-0637(94)90007-8.

Picheral, M, Guidi, L, Stemmann, L, Karl, DM, Iddaoud, G, Gorsky, G. 2010. The Underwater Vision Profiler 5: An advanced instrument for high spatial resolution studies of particle size spectra and zooplankton. *Limnology and Oceanography: Methods* **8**(9): 462–473. DOI: http://dx.doi.org/10.4319/lom.2010.8.462.

Prairie, JC, Montgomery, QW, Proctor, KW, Ghiorso, KS. 2019. Effects of phytoplankton growth phase on settling properties of marine aggregates. *Journal of Marine Science and Engineering* **7**(8): 265. DOI: http://dx.doi.org/10.3390/jmse7080265.

Randelhoff, A, Oziel, L, Massicotte, P, Bécu, G, Galí, M, Lacour, L, Dumont, D, Vladoiu, A, Marec, C, Bruyant, F. 2019. The evolution of light and vertical mixing across a phytoplankton ice-edge bloom. *Elementa Science of the Anthropocene* **7**: 20. DOI: http://dx.doi.org/10.1525/elementa.357.

Ras, J, Claustre, H, Uitz, J. 2008. Spatial variability of phytoplankton pigment distributions in the Subtropical South Pacific Ocean: Comparison between in situ and predicted data. *Biogeosciences* **5**(2): 353–369.

Reigstad, M, Wassmann, P. 2007. Does *Phaeocystis* spp. contribute significantly to vertical export of organic carbon? *Biogeochemistry* **83**: 217–234.

Riebesell, U. 1991. Particle aggregation during a diatom bloom. II. Biological aspects. *Marine Ecology Progress Series* **69**: 281–291.

Riebesell, U. 1993. Aggregation of *Phaeocystis* during phytoplankton spring blooms in the southern North Sea. *Marine Ecology Progress Series* **96**(3): 281–289.

Riebesell, U, Reigstad, M, Wassmann, P, Noji, T, Passow, U. 1995. On the trophic fate of *Phaeocystis pouchetii* (Hariot): VI. Significance of *Phaeocystis*-derived mucus for vertical flux. *Netherlands Journal of Sea Research* **33**(2): 193–203.

Rousseau, V, Mathot, S, Lancelot, C. 1990. Calculating carbon biomass of *Phaeocystis* sp. from microscopic observations. *Marine Biology* **107**(2): 305–314. DOI: http://dx.doi.org/10.1007/BF01319830.

Rousseaux, C, Gregg, W. 2013. Interannual variation in phytoplankton primary production at a global scale. *Remote Sensing* **6**(1): 1–19. DOI: http://dx.doi.org/10.3390/rs6010001.

Saint-Béat, B, Fath, BD, Aubry, C, Colombet, J, Dinasquet, J, Fortier, L, Galindo, V, Grondin, P-L, Joux, F, Lalande, C. 2020. Contrasting pelagic ecosystem functioning in eastern and western Baffin Bay revealed by trophic network modeling. *Elementa: Science of the Anthropocene* **8**: 1. DOI: http://dx.doi.org/10.1525/elementa.397.

Sanmartín, P, Villa, F, Silva, B, Cappitelli, F, Prieto, B. 2011. Color measurements as a reliable method for estimating chlorophyll degradation to phaeopigments. *Biodegradation* **22**(4): 763–771.

Sarthou, G, Timmermans, KR, Blain, S, Tréguer, P. 2005. Growth physiology and fate of diatoms in the ocean: A review. *Journal of Sea Research* **53**(1–2): 25–42. DOI: http://dx.doi.org/10.1016/j.seares.2004.01.007.

Schmid, MS, Fortier, L. 2019. The intriguing co-distribution of the copepods *Calanus hyperboreus* and *Calanus glacialis* in the subsurface chlorophyll maximum of Arctic seas. *Elementa: Science of the Anthropocene* **7**(1). DOI: http://dx.doi.org/10.1525/elementa.388.

Schoemann, V, Becquevort, S, Stefels, J, Rousseau, V, Lancelot, C. 2005. *Phaeocystis* blooms in the global ocean and their controlling mechanisms: A review. *Journal of Sea Research* **53**(1–2): 43–66.

Screen, JA, Simmonds, I. 2010. The central role of diminishing sea ice in recent Arctic temperature amplification. *Nature* **464**(7293): 1334.

Shanks, AL, Walters, K. 1997. Holoplankton, meroplankton, and meiofauna associated with marine snow. *Marine Ecology Progress Series* **156**: 75–86.

Slagstad, D, Støle-Hansen, K. 1991. Dynamics of plankton growth in the Barents Sea: Model studies. *Polar Research* **10**(1): 173–186.

Smetacek, V. 1999. Diatoms and the ocean carbon cycle. Protist **150**(1): 25–32.

Smith, WO. 1994. Primary productivity of a *Phaeocystis* bloom in the Greenland Sea during Spring, 1989. *Washington DC American Geophysical Union Geophysical Monograph Series* **85**: 263–272. DOI: http://dx.doi.org/10.1029/GM085p0263.

Smith, WO, Codispoti, LA, Nelson, DM, Manley, T, Buskey, EJ, Niebauer, HJ, Cota, GF. 1991. Importance of *Phaeocystis* blooms in the high-latitude ocean carbon cycle. *Nature* **352**(6335): 514–516. DOI: http://dx.doi.org/10.1038/352514a0.

Søreide, JE, Carroll, ML, Hop, H, Ambrose Jr, WG, Hegseth, EN, Falk-Petersen, S. 2013. Sympagic-pelagic-benthic coupling in Arctic and Atlantic waters around Svalbard revealed by stable isotopic and fatty acid tracers. *Marine Biology Research* **9**(9): 831–850.

Søreide, JE, Falk-Petersen, S, Hegseth, EN, Hop, H, Carroll, ML, Hobson, KA, Blachowiak-Samolyk, K. 2008. Seasonal feeding strategies of *Calanus* in the high-Arctic Svalbard region. *Deep Sea Research Part II: Topical Studies in Oceanography* **55**(20–21): 2225–2244.

Søreide, JE, Leu, EVA, Berge, J, Graeve, M, Falk-Petersen, S. 2010. Timing of blooms, algal food quality and *Calanus glacialis* reproduction and growth in a changing Arctic. *Global Change Biology* **16**(11): 3154–3163.

Steinberg, DK. 1995. Diet of copepods (*Scopalatum vorax*) associated with mesopelagic detritus (giant larvacean houses) in Monterey Bay, California. *Marine Biology* **122**(4): 571–584.

Stroeve, J, Holland, MM, Meier, W, Scambos, T, Serreze, M. 2007. Arctic sea ice decline: Faster than forecast. *Geophysical Research Letters* **34**: L09501. DOI: http://dx.doi.org/10.1029/2007GL029703.

Tang, CC, Ross, CK, Yao, T, Petrie, B, DeTracey, BM, Dunlap, E. 2004. The circulation, water masses and sea-ice of Baffin Bay. Progress in Oceanography **63**(4): 183–228.

Taucher, J, Stange, P, Algueró-Muñiz, M, Bach, LT, Nauendorf, A, Kolzenburg, R, Büdenbender, J, Riebesell, U. 2018. In situ camera observations reveal major role of zooplankton in modulating marine snow formation during an upwelling-induced plankton bloom. *Progress in Oceanography* **164**: 75–88. DOI: http://dx.doi.org/10.1016/j.pocean.2018.01.004.

Tedesco, L, Vichi, M, Scoccimarro, E. 2019. Sea-ice algal phenology in a warmer Arctic. *Science Advances* **5**(5): eaav4830. DOI: http://dx.doi.org/10.1126/sciadv.aav4830.

Torres-Valdés, S, Tsubouchi, T, Bacon, S, Naveira-Garabato, AC, Sanders, R, McLaughlin, FA, Petrie, B, Kattner, G, Azetsu-Scott, K, Whitledge, TE. 2013. Export of nutrients from the Arctic Ocean. *Journal of Geophysical Research: Oceans* **118**(4): 1625–1644.

Toullec, J, Vincent, D, Frohn, L, Miner, P, Le Goff, M, Devesa, J, Moriceau, B. 2019. Copepod grazing influences diatom aggregation and particle dynamics. *Frontiers in Marine Science* **6**. DOI: http://dx.doi.org/10.3389/fmars.2019.00751.

Tremblay, C, Runge, JA, Legendre, L. 1989. Grazing and sedimentation of ice algae during and immediately after a bloom at the ice-water interface. *Marine Ecology Progress Series* **56**(3): 291–300.

Tremblay, J-É, Anderson, LG, Matrai, P, Coupel, P, Bélanger, S, Michel, C, Reigstad, M. 2015. Global and regional drivers of nutrient supply, primary production and CO_2 drawdown in the changing Arctic Ocean. *Progress in Oceanography* **139**: 171–196. DOI: http://dx.doi.org/10.1016/j.pocean.2015.08.009.

Tremblay, J-É, Gratton, Y, Carmack, EC, Payne, CD, Price, NM. 2002. Impact of the large-scale Arctic circulation and the North Water Polynya on nutrient inventories in Baffin Bay. *Journal of Geophysical Research: Oceans* **107**(C8): 26-1-26-14. DOI: http://dx.doi.org/10.1029/2000JC000595.

Tremblay, J-É, Michel, C, Hobson, KA, Gosselin, M, Price, NM. 2006. Bloom dynamics in early opening waters of the Arctic Ocean. *Limnology and Oceanography* **51**(2): 900–912. DOI: http://dx.doi.org/10.4319/lo.2006.51.2.0900.

Turner, JT. 2015. Zooplankton fecal pellets, marine snow, phytodetritus and the ocean's biological pump. Progress in Oceanography **130**: 205–248. DOI: http://dx.doi.org/10.1016/j.pocean.2014.08.005.

Utermöhl, H. 1958. Zur Vervollkomnung der quantitativen Phytoplankton-Methodik. *Mitteilungen der internationale Vereinigung für theoretische und angewandte Limnologie* **9**: 1–38.

Vancoppenolle, M, Meiners, KM, Michel, C, Bopp, L, Brabant, F, Carnat, G, Delille, B, Lannuzel, D,

Madec, G, Moreau, S. 2013. Role of sea ice in global biogeochemical cycles: Emerging views and challenges. *Quaternary Science Reviews* **79**: 207–230.

Vihma, T. 2014. Effects of Arctic sea ice decline on weather and climate: A review. *Surveys in Geophysics* **35**(5): 1175–1214.

Vilgrain, L, Maps, F, Picheral, M, Babin, M, Aubry, C, Irisson, JO, Ayata, SD. 2021. Trait-based approach using in situ copepod images reveals contrasting ecological patterns across an Arctic ice melt zone. *Limnology and Oceanography* **66**(4): 1155–1167. DOI: http://dx.doi.org/10.1002/lno.11672.

Waite, AM, Olson, RJ, Dam, HG, Passow, U. 1995. Sugar-containing compounds on the cell surfaces of marine diatoms measured using concanavalin *a* and flow cytometry. *Journal of Phycology* **31**(6): 925–933. DOI: http://dx.doi.org/10.1111/j.0022-3646.1995.00925.x.

Wassmann, P, Duarte, CM, Agusti, S, Sejr, MK. 2011. Footprints of climate change in the Arctic marine ecosystem. *Global Change Biology* **17**(2): 1235–1249.

Wassmann, P, Ratkova, T, Andreassen, I, Vernet, M, Pedersen, G, Rey, F. 1999. Spring bloom development in the marginal ice zone and the central Barents Sea. *Marine Ecology* **20**(3–4): 321–346. DOI: http://dx.doi.org/10.1046/j.1439-0485.1999.2034081.x.

Zhang, J, Spitz, YH, Steele, M, Ashjian, C, Campbell, R, Berline, L, Matrai, P. 2010. Modeling the impact of declining sea ice on the Arctic marine planktonic ecosystem. *Journal of Geophysical Research: Oceans* **115**(C10): 1–24.

ELEMENTA
Science of the Anthropocene

Elem Sci Anth is a peer-reviewed open access journal published by University of California Press.

OPEN ACCESS